
NeuroChaT: A Toolbox to Analyse the Dynamics of Neuronal Encoding in Freely-Behaving Rodents *in vivo*

Md Nurul Islam¹, Seán K. Martin¹, John P. Aggleton², Shane M. O'Mara^{1*}

¹ School of Psychology and Institute of Neuroscience, Trinity College Dublin, Dublin 2, Republic of Ireland

² School of Psychology, Cardiff University, Cardiff, United Kingdom

* **For correspondence:** smomara@tcd.ie (SMOM)

Abstract

There is a dearth of freely-available, standardised open source analysis tools available for the analysis of neuronal signals recorded *in vivo* in the freely-behaving animal. In response, we have developed a freely-available, open-source toolbox, NeuroChaT (Neuron Characterisation Toolbox), specifically addressing this lacuna. Although we have particularly emphasised single unit analyses for spatial coding, NeuroChaT also characterises rhythmic properties of units and their dynamics associated with local field potential signals. NeuroChaT was developed using Python and facilitates a complete pipeline from automation of analysis to producing and managing publication-quality figures. Additionally, we have adopted a platform-independent format (Hierarchical Data Format version 5) for storing recorded and analysed data. By providing an easy-to-use software package, we aim to simplify the adoption of standardised analyses for behavioural neurophysiology and facilitate open data sharing and collaboration between laboratories.

Keywords

Cognitive map, data analysis, spatial coding, single unit, open software, electrophysiology

1 Introduction

2 Where and how spatial information is represented in the brain has been of great scientific interest
3 since O’Keefe & Dostrovsky [1] first described the spatially-receptive fields of hippocampal
4 neurons (since named ‘place cells’). Subsequently, many spatially-responsive cell types have been
5 described, including head direction cells [2, 7], grid cells (neurons with multiple receptive fields
6 arranged in a triangular grid) [9, 12], as well as boundary cells and object cells (neurons that
7 respond to objects placed in the environment) [27, 28]. Moreover, neurons tuned to non-spatial,
8 natural stimuli (e.g. speed cells), have also been described, and are likely to contribute to the
9 dynamic representations of ‘self-location’, such as for path integration [29, 34].

10 Standardised methods have evolved for studying the spatial selectivity of neurons in the
11 freely-behaving animal. Briefly, rats (or mice) are surgically implanted with recording electrodes
12 targeted at a particular brain region or regions. After post-surgery recovery, the freely-moving
13 rat traverses mazes or open fields (often in search of food). The experimental apparatus may be
14 shielded from the larger laboratory by curtains, to control the local cue set. This cue set may
15 be manipulated with, for example, cue rotations or selective cue deletions. Neuronal activity
16 (action potentials, or ‘spikes’) is recorded, amplified, time-stamped and correlated with the
17 moment-to-moment position of the rat. These correlations are used to generate colour-coded
18 contour maps representing the density of spike firing at all points occupied by the rat. Under
19 these conditions, many hippocampal neurons fire in a locally defined area of the maze (usually
20 no more than a few percent of the total maze area) and remain silent or fire at low rates (<1 Hz)
21 in other areas of the maze [34].

22 Modern recording techniques may use multiple recording fine-wire electrodes or electrodes
23 based on printed circuit technology [35]. These approaches generate vast amounts of data,
24 particularly if acquired over long duration recording sessions. Moreover, advances in the design
25 of recording electrodes have increased the number of recording sites [22, 35], increasing data
26 volumes [19, 30]. Analysing such large data sets involves:

- 27 1. Identifying the activity of single neurons from the noisy recorded data, known as spike
28 sorting [21].
- 29 2. Analysing relationships between spatial and non-spatial variables and verifying correlations.
- 30 3. Assessing individual neurons and computing inferential statistics to describe local popula-
31 tions.

32 There are some open-source software packages for studying the neural codes of single neurons,
33 multiple neurons, and local field potentials [15, 33]. Many individual laboratories use custom-
34 written software, but there is no software package widely available implementing standardised
35 algorithms for spatial and non-spatial neuronal coding within one working environment, thereby
36 limiting wider adoption of *in vivo* electrophysiological recording methods. Nor is there a widely-
37 and freely-available toolbox to analyse neuronal encoding of spatial and non-spatial information
38 that also incorporates batch processing of substantial amounts of data. Finally, available
39 packages do not often easily facilitate quick implementation and integration of new techniques
40 along with established ones given the challenges associated with the evolution of new technology.

41 To address this important lacuna, we have developed a toolbox, NeuroChaT (Neuron
42 Characterisation Toolbox), a graphical user interface (GUI)-based open-source software that
43 brings together peer-reviewed analysis methods in a unified framework for greater accessi-
44 bility and to provide an easier implementation of analyses. We have adopted the widely-
45 used platform-independent Hierarchical Data Format version 5 (HDF5) for storing recorded
46 and analysed data, which is compatible with most common programming languages. Neu-
47 roChaT provides a systematic approach for analysing large numbers of neurons and man-
48 aging the graphical and parametric outputs. NeuroChaT is freely available from GitHub
49 (<https://github.com/shanemomara/omaraneneuro1ab>) under the GNU General Public License

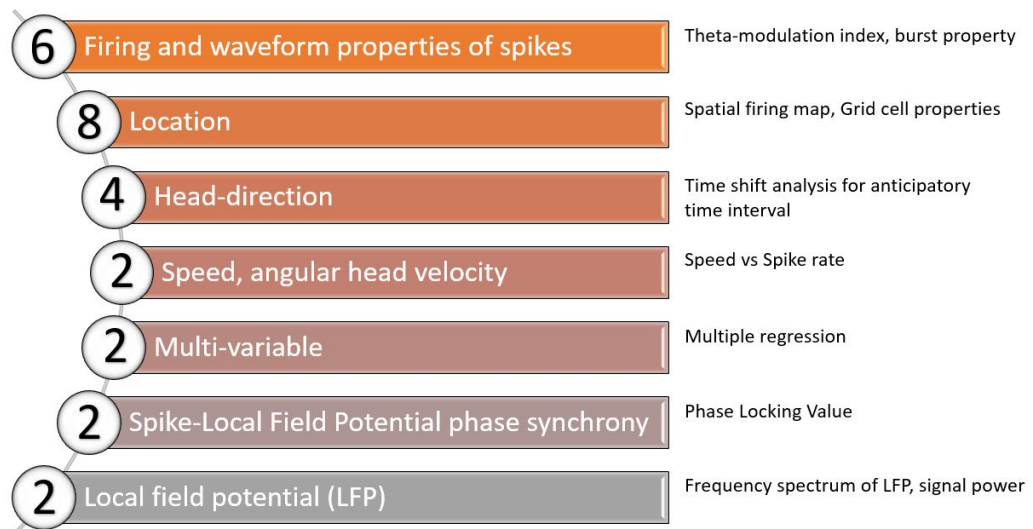


Figure 1. The number of methods available in NeuroChaT for each category of analysis.

50 (v3.0) for non-commercial use and open source development. Sample data, a GUI user tutorial
 51 and extensive application programming interface (API) documentation are also provided on
 52 the project website. We hope NeuroChaT will enable standardisation of analyses and assist in
 53 developing novel algorithms and experimental designs through its ease of analysis based on a
 54 widely-used and standardised data format.

55 Methods

56 Analysis methods

57 NeuroChaT consists of multiple analysis methods that produce graphical figures and numerical
 58 results based on the normative neuronal rate coding scheme, where changes in firing rate
 59 represent responses to a stimulus or stimuli. The methods that are available in NeuroChaT are
 60 enumerated in Figure 1 and some example graphical outputs are shown in Figure 2.

61 NeuroChaT provides six analysis methods for assessing the waveform and firing properties
 62 of single units. Waveform properties measure characteristics such as the mean wave amplitude
 63 and width on each tetrode in a recording. The inter-spike interval (ISI), ISI autocorrelation,
 64 and cell bursting properties are calculated from the spike train of the single unit. In addition, a
 65 theta-modulated cell index and theta-skipping cell index for the single unit are both calculated
 66 by fitting an oscillating curve to the ISI autocorrelation histogram.

67 NeuroChaT offers eight spatial locational analyses. The spatial path of the subject and the
 68 spike train are used to produce a locational firing rate map. From the firing rate map, place
 69 field, grid cell, border cell, and gradient cell analyses are available. The place field is determined
 70 by finding the connected area of activity in the arena with the highest firing rate. Grid cell
 71 analysis involves calculating the spatial autocorrelation of the firing rate map and assessing the
 72 shape formed by the peaks in autocorrelation. For border cell analyses, a border of the arena is
 73 estimated from the path the animal traversed and the firing rate is compared to the distance
 74 from the border. Gradient cell analysis begins similarly to border cell analysis and then fits a
 75 Gompertz function (a monotonically increasing function that exhibits a slow growth rate at
 76 the border and the centre of the arena) to the relationship between firing rate and the distance
 77 from the border.

78 The following three methods are shared between spatial locational and head directional

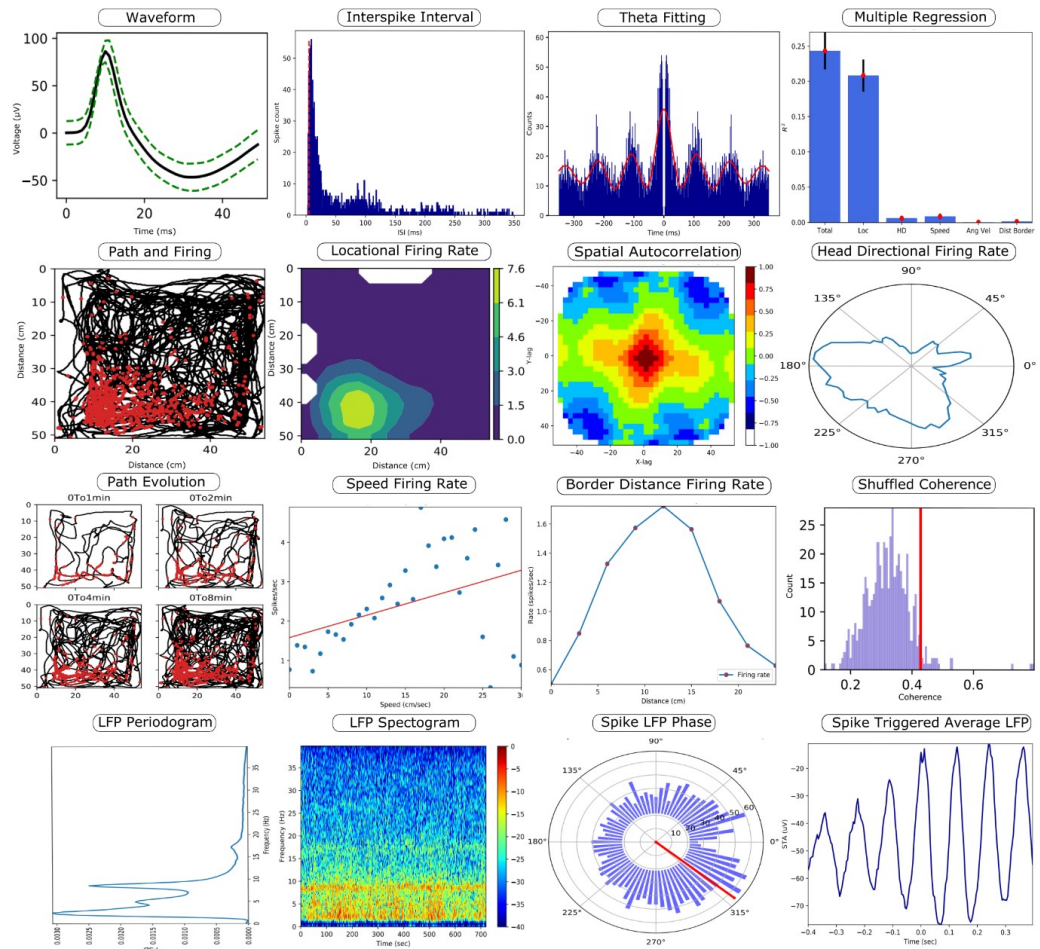


Figure 2. Example plots to demonstrate the graphical output from a subset of the analyses available in NeuroChaT. A short description of each plot follows, going from top left to bottom right and moving along rows. (1) The mean waveform of a single unit (black) and the standard deviation of the waveform (green). (2) The histogram of the interspike interval of a unit, with the red dotted line showing the refractory period. (3) A wave fitted to the autocorrelation of the interspike interval at theta frequency (8 Hz). (4) The predictive power of location, head direction, speed, angular velocity, and border distance for the firing rate. (5) The path of the rodent in a square arena (black) and firing (red). (6) The locational firing rate information modulated by dwell time in the arena, with green indicating high firing rates. (7) The spatial autocorrelation of the locational firing rate map, with red indicating high spatial autocorrelation. (8) A polar plot showing the firing rate modulated by head direction. (9) The path of the animal in the arena and firing activity over time. (10) A scatter plot of speed against the firing rate, with the red line showing a line of best fit. (11) A line plot comparing the border distance to the firing rate. (12) A histogram of spatial coherence values for 500 shuffled spike trains, with the red line indicating the 95th percentile value. (13) The power in the local field potential (LFP) signal at different frequencies. (14) The power of the LFP signal at different frequencies over time, with red indicating high power values. (15) A polar plot of the LFP phase value at each spike time, with the red line indicating the mean phase. (16) The average LFP signal around the time of a spike occurrence.

79 analyses. Time-lapse analyses examine the evolution of the firing rate over time to determine
80 if spatial tuning occurs during the animal’s exploration of the environment. Shuffling tests
81 randomly distribute the original spikes along the path of the animal to investigate whether
82 the effect of a spatial variable on the firing rate of a unit has occurred by chance. Time-shift
83 analyses gradually move the whole spike train of a unit forwards and backwards in time to
84 test if there is a corresponding gradual change in the coding specificity, indicating a systematic
85 variation in the firing rate and providing timing information of the spatial cells [6]. Skaggs
86 information content [3] is available in NeuroChaT for any spatial variable and is appropriate to
87 use in combination with these spike time-altering analyses. Furthermore, for locational analyses,
88 these methods can be used in combination with coherency and sparsity measures, which assess
89 the spatial quality of a single unit. For head directional analyses, these methods can be used
90 with the Rayleigh Z-score and the concentration parameter for the von Mises distribution, which
91 assess the uniformity of the head-direction firing rate.

92 Head directional firing rate analyses are also available. These compare the spike train
93 information to the head direction of the animal and can be computed for different angular
94 velocities, such as when the animal is turning clockwise or counterclockwise. To round off
95 NeuroChaT’s single variable spatial analysis toolkit, there are two analyses methods related to
96 speed and angular velocity. In these, the spike rate is linearly correlated to the speed of the
97 animal and the angular velocity of the animal’s head in both the clockwise and counter-clockwise
98 directions.

99 There are two multi-variable spatial analyses in NeuroChaT. The first involves building a
100 multi-variable linear regression model to predict the firing rate of a single unit. The location,
101 head direction, speed, angular velocity, and distance to the border are the five predictor variables
102 used to estimate the firing rate of the unit at multiple binned points in time. The predictive
103 power of these variables is indicative of the spatial tuning of the single unit. The second analysis
104 compares the observed firing rate related to an independent variable (speed, angular velocity,
105 distance to the border, or head direction) to an estimated firing rate. The estimated firing rate
106 is formed solely from the binned locational firing rate map and the value of the independent
107 variable in each locational bin. In this way, it can be determined if modulation of the firing rate
108 by an independent variable is a real effect, or if it is attributable to an inhomogeneous sampling
109 of the independent variable.

110 There are two analysis methods available in NeuroChaT to analyse the raw local field
111 potential (LFP) signal. The first involves computing the time-resolved frequency spectrum of
112 the LFP. The second involves computing the average power in the LFP over the duration of the
113 recording in the different frequency bands, such as the Theta band, using Welch’s periodogram.
114 When considering the LFP in relation to the spiking information, two analyses are available.
115 In the first analysis, the spike-triggered average LFP signal, the phase-locking value, and the
116 spike-field coherence measures are obtained to assess the phase-locking of a unit to the LFP
117 signals. In the second analysis, the distribution of the phase in the LFP at which spikes occur is
118 formed by using the Hilbert Transform of the band-pass filtered LFP signal.

119 In addition to the analyses listed in Figure 1, two uncategorised methods are available in
120 NeuroChaT. NeuroChaT can compute the Hellinger distance and the Bhattacharyya coefficient
121 between spike clusters to evaluate the separation of unit clusters on a tetrode or to compare the
122 similarity of a cluster across recordings. The latter can be used to help identify if the same cell
123 is present in multiple recordings. To aid analysing substantial amounts of data, NeuroChaT can
124 produce a summary png plot of the spatial information on each tetrode in multiple recordings.
125 For Axona data, this can recursively search directories and produce a summary for any tetrode
126 file with sorted spikes and is readily extendable to other formats.

127 **Implementation**

128 NeuroChaT uses object-oriented programming (OOP), using the freely-available open-source
129 programming language, Python. In OOP, classes are programming elements that work as

130 a placeholder for data and functions an object can perform, providing encapsulation of its
 131 attributes and actions. The relationships between the classes are shown in Figure 3 using class
 132 diagrams. The classes were designed to encapsulate one aspect of the software. For example, the
 133 NeuroChaT UI class manages the GUI and corresponding interactions between the graphical
 134 elements with the underlying code and data containers.

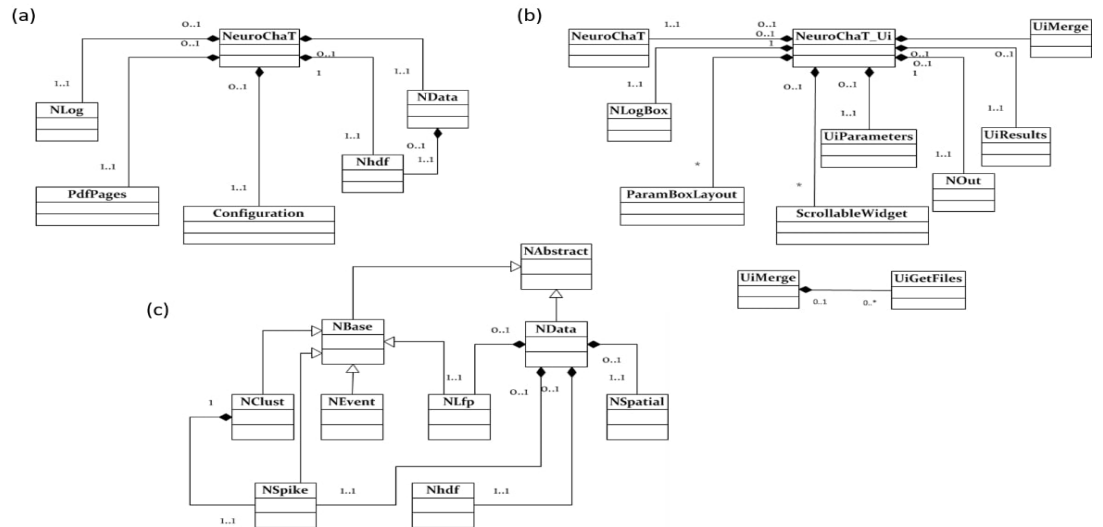


Figure 3. Class diagrams showing the relationships between the classes in NeuroChaT. Although each class contains several member attributes and local variables, these are not represented to keep the diagrams compact. The regular white arrows indicate class inheritance while the black diamond arrows indicate object composition. The numbers along an arrow specify the allowable number of instances in the relationship. For example, in the composition between NData and Nhdf, 1..1 indicates that an NData object has exactly one Nhdf object, while 0..1 indicates that an Nhdf object belongs to at most one NData object.

135 NeuroChaT class (NeuroChaT)

136 The NeuroChaT class takes information from GUI, determines what analysis or action to perform,
 137 and dictates to other connected classes to act accordingly. NData is a façade data structure
 138 composed of data classes and governs information flow between the other data classes, namely
 139 NSpike, NSpatial, NLfp and Nhdf. Data classes, like NSpike and NSpatial, are placeholders
 140 for spiking activity of neurons and the spatial position of the animal, respectively. NeuroChaT
 141 passes the relevant parameters to NData, and asks permission to perform the analyses, on a
 142 cell-by-cell basis, based on the user input in the specification phase.

143 User interface class (NeuroChaT_UI)

144 The NeuroChaT user interface class is the graphical component of the NeuroChaT software. It
 145 provides the interface for users to specify the analyses they want to perform, select the data
 146 and parameters for those analyses, and, finally, the graphical file format to store the results in.
 147 This is a simple-to-use, tick-box interface with features that enable settings and information
 148 to be forwarded to the NeuroChaT object. Its composing objects are all graphical elements,
 149 except the NeuroChaT object. Although built in a composite structure, this class is static, in
 150 the sense that its components cannot be altered dynamically using commands outside of the
 151 class itself. Therefore, the coupling between these classes to others is considered tight, and any
 152 changes required must involve changing the code file where the class is defined.

153 **Neuronal spiking information class (NSpike)**

154 The NSpike class is the container for neuronal spiking activities. It decodes the files that record
155 the waveforms and timestamps of the spikes from a proprietary format and stores these in a
156 Neurodata Without Borders (NWB) format. It also contains analyses involving spiking activity
157 of the single-units, i.e. inter-spike interval, assessing rhythmicity etc., along with implementing
158 the decoders for the copyrighted data formats. If the recording undergoes spike-sorting, this class
159 also provides the information about which spike-waveform belongs to which putative neuron.

160 **Neuronal local field potential class (NLfp)**

161 The NLfp class is the container for recorded LFP activities. The timestamps and the amplitude
162 of the LFP information are stored in the instance of this class along with other recording
163 information, i.e. LFP channel number or the bandwidth of the filter that was used to extract
164 the LFP signal from the recorded data. The analyses that are implemented in the class are
165 frequency spectrum of the LFP signal, LFP phase distribution, phase locking and SFC of an
166 event-timestamp train as that of a single-unit, event-triggered average LFP signal etc.

167 **Spatial information class (NSpatial)**

168 The NSpatial class contains methods for analysing the spatial correlation of the single units.
169 The only single unit information required for this class is the timing of the activity. This is
170 passed directly as an input to its methods (API use guide) or through NData. When used with
171 the NData class, it receives the information through that class instead of coupling directly to
172 the NSpike data. This creates a layer of independence between the data classes and reduces the
173 effort required to couple them.

174 **Neuronal spike sorting class (NClust)**

175 The NClust class provides the waveform features, unit spiking activity, and measures of cluster
176 separation for quality assessment of spike-sorting and measuring the cluster similarity with
177 a unit in another NClust object. The class delegates the handling of the file containing the
178 neuronal spike information to the NSpike object that is an attribute of the NClust instance.

179 **Neuronal Hierarchical Data Format class (Nhdf)**

180 NData also contains an Nhdf data object to provide read/write access of HDF5 files containing
181 spatial or neural data within the class without decoding the proprietary file formats every time
182 the data is loaded. As the HDF5 file contains all the data, it makes storage more manageable
183 through a readable format. Nhdf contains methods to read and write what is called groups and
184 datasets in HDF5 file format. It also contains methods that are specific to storing individual
185 NSpike, NLfp, and NSpatial data to their common HDF5 container for a recording session.
186 NeuroChaT creates one such file for each recording session, not for individual units or electrodes.

187 **Neuro-data class (NData)**

188 The NData object, as shown in Figure 3, comprises data objects of different kinds, and is
189 built upon the composite structural object pattern [4]. This type of design pattern used in
190 NeuroChaT creates a modular structure and allows the objects to alter dynamically without
191 intense refactoring of the code. In NeuroChaT, NAbstract and NBase form the parent classes
192 with basic and common methods and attributes across different data types. Each data class
193 representing the neural data (NSpike, NClust, NLfp), along with the event class NEvent, inherits
194 NBase, where NBase itself inherits NAbstract and extends its capabilities. The NSpatial class
195 inherits the NAbstract class. The NData class gets one instance or object for each NSpatial,

196 NSpike and NLfp class as its attribute. The rationale behind this design is to provide an
197 encapsulation of the interaction among the behavioural and neural data types, i.e. how the peers
198 like NSpatial and NSpike would know each other. Either they will need to have a reference to
199 each other, which increases their coupling, or they need to be cooperated using another object,
200 which, in our design, is the NData object.

201 A similar design principle is also followed in other composite classes of NeuroChaT. The
202 getter and setter methods of the composite class instance then allow dynamically changing the
203 objects or retrieving it. For example, the spatial data does not need to be changed for a single
204 recording while analysing for multiple single units recorded in the same session. Therefore, the
205 NSpatial object remains the same, but the data in the NSpike object changes with changing the
206 units. Now, creating one instance of NData for every pair of spatial and single unit data is not
207 very memory efficient. Instead, we can replace the data in the NSpike by reloading the spike
208 file while it is still a member of the NData object and optimise the reuse of data objects, save
209 memory, and increase the performance of the software.

210 **Experimental event class (NEvent)**

211 NEvent class implements event-related data management and basic analyses, i.e. peri-stimulus
212 time histogram (PSTH) and analyses pertaining to locking of the LFP signals to the event(s).
213 It also delegates the analyses to the relevant NSpike or NLfp objects. For example, if the PSTH
214 is to be obtained from a spike-train, the NEvent object recruits the relevant NSpike and uses its
215 function computes the same analysis.

216 **Visualisation and export**

217 NeuroChaT uses a custom python module ‘nc_plot’ to plot the graphical outcomes of the
218 analyses, then stores the parametric results in a tabular format and converts the data into the
219 standardised HDF5 files using the Nhdf() object. The user can perform statistical analyses
220 on the parametric results if required: this is the Inference phase of the data analysis workflow
221 using NeuroChaT. The specifications of the data, analyses, and input parameters can be saved
222 for future use in an ‘ncfg’ (NeuroChaT configuration) file. This file is in YAML format, a
223 human-readable data-serialisation format commonly used for configuration files.

224 **Utility classes**

225 In addition to the primary classes already described, NeuroChaT also provides classes that
226 provide essential utility functionality. NLogBox is an editable graphical widget that is subclassed
227 from QTextEdit of the QtWidgets of PyQt5 to format the logged messages into HTML format.
228 ParamBoxLayout is derived from QVBoxLayout and is used for arranging the parameter
229 definition in a vertical layout in the Settings menu of the interface. ScrollableWidget provides a
230 container of listed items so the user can scroll through the items if the list takes more space
231 than the widget they are located in. UiParameters define and add the graphical elements to
232 the interface. NOut replaces the standard output texts of Python or IPython (print command)
233 into texts that are received by the logger of the system. UiResults is a sub-class of QDialog of
234 QtWidgets that displays the results of the analysis in a tabular format along with an option to
235 export them in an Excel file. UiMerge is a graphical window that asks the user to select a list
236 of pdf filenames to merge them into one file or to transfer to a single folder. The user can also
237 select the pdf files manually using an interactive window built in UiGetFiles class.

238 **Operation**

239 NeuroChaT has been tested to run on Windows 7, Windows 10, and Ubuntu 18.04. NeuroChaT
240 requires 100MB of system storage to perform a full install, including Python and Python package

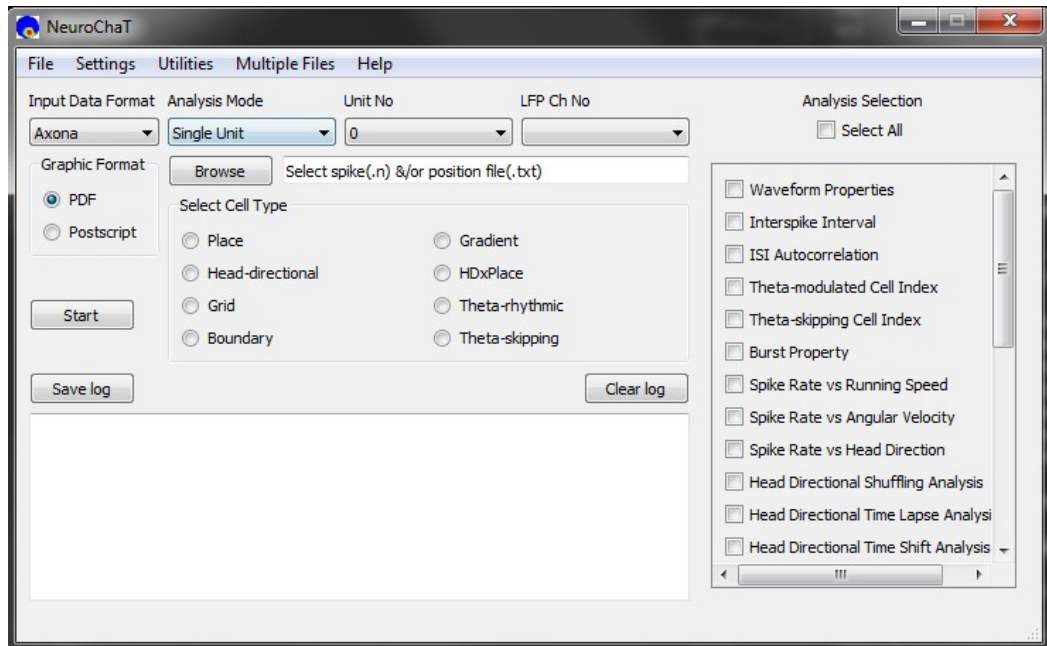


Figure 4. The graphical user interface to NeuroChaT.

241 dependencies. There are no system requirements to run NeuroChaT, but at least 8GB of RAM
 242 is recommended.

243 The NeuroChaT graphical user interface (GUI) is shown in Figure 4. The linear workflow
 244 for using NeuroChaT is shown in Figure 5. Initial analysis specification starts with the selection
 245 of data, analysis techniques to be used, and input parameters for the analyses, using the GUI.
 246 This set of choices is collectively referred to as the ‘configuration’. This selection is passed to
 247 the NeuroChaT backend, which then computes the specific analyses, and automatically plots
 248 and stores the graphical results to the storage disk. At the end of the analysis, a graphical table
 249 pops up showing the numerical results that the user can refer to for inferential analysis. These
 250 numerical outputs can be exported to an excel file, while graphical results are exported to a
 251 PDF file. NeuroChaT can store a specific configuration to be loaded again at a later date using
 252 the GUI.

253 **Batch-mode analysis**

254 NeuroChaT facilitates batch mode processing by providing the unit and spatial information in
 255 an Excel list. Researchers often keep track of identified single units or units of interest using an
 256 Excel file; we facilitate this analysis using this list. The output graphics are, accordingly, all
 257 stored in the respective data folder. Units with speculated-upon similar properties, for example,
 258 head-directional firing, can be listed in one file for the convenience of post hoc inferential analysis
 259 of population data. The verification utility in the software can verify the information specified
 260 in the Excel list for batch processing, i.e. whether the specified path or files exist, or whether
 261 the cluster unit of interest belongs to the recording or is mistyped. This ensures the user does
 262 not waste time finding issues after running the analyses and knows ahead of about problematic
 263 specifications. As many of the NeuroChaT analyses are time consuming, this is a convenient
 264 way of eliminating common human errors and reduces time wasted.

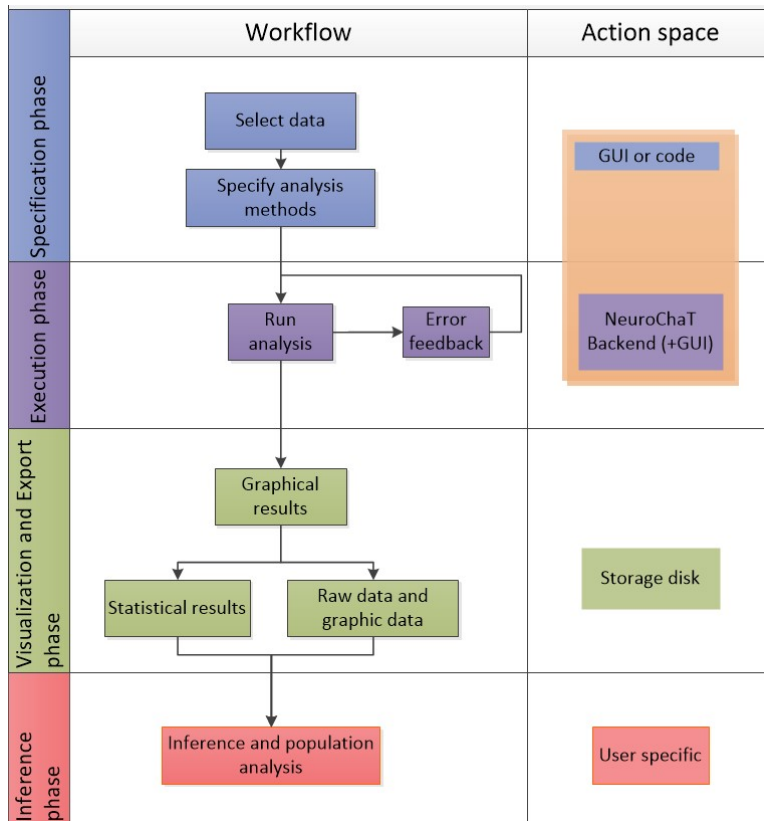


Figure 5. Linear workflow for using NeuroChaT.

265 Nomenclature

266 NeuroChaT provides for better data management by standardising the nomenclature in its
267 output data file. It creates a unique name for each unit of a recording session using the following
268 format: `unit_id = record_id+ 'TT'+ tet_no+ '_SS.'` + `unit_no + '.'+ eeg_file_ext` where `record_id`
269 = unique file or folder identifier for each recording session used to store and identify data,
270 `tet_no` = electrode number where the unit is identified, `unit_no` = tag of the unit or the cluster
271 number in spike-sorting, `eeg_file_ext` = filename or the extension used for naming an LFP data
272 file. This approach brings efficiency to managing and scrutinising the outcome of data analyses.
273 Current analyses in NeuroChaT can produce more than 50 graphical outputs for each unit with
274 publication-quality images. Storing them in one file creates the initial layer of output data
275 management. These output files are stored in the respective data folder, so they can be easily
276 traced. The unique name 'unit_id.pdf' of the unit information is essential when working with
277 many such units from the same study; otherwise, keeping track of the output graphics would be
278 overwhelming in terms of the number of graphics files and the amount of disk space they would
279 require.

280 Converting data to a widely-accessible format

281 The proprietary format data are converted into HDF5 and are accessible through the HDF5
282 file viewers (www.hdfgroup.org/), once they go through NeuroChaT. Every time NeuroChaT
283 analyses a unit, it stores the analysed data in the HDF5 file as a group that has been named
284 following the NeuroChaT convention described above. There is always one HDF5 file for one
285 recording session but different groups for each recorded unit. The recorded data are stored
286 following the specification as in the NWB format [31]. NeuroChaT also has a utility that
287 converts the unit data from a vendor format to HDF5 format using a data specification list like
288 the one used for the batch-mode processing. Additionally, the NeuroChaT input output module
289 for HDF5 through Nhd5 enables writing data and attributes to any of its paths or data without
290 rewriting the entire file which was a major limitation in the NWB API.

291 Utility for graphics management

292 Given that many units are recorded over time, the number of pdf or ps output files grows linearly.
293 The PDF management utility in NeuroChaT facilitates merging the output files of interesting
294 units into one file or moving them to a folder to group them together. The utility can be used
295 either by providing a list of units or by manually choosing the files using an interactive window.
296 At the end of each execution, NeuroChaT provides a list of pdf files where the graphical outputs
297 for each analysed unit are stored. Users can export this list from the GUI utility menu and can
298 use the list for merging or accumulating them into one folder. Thus, NeuroChaT also bridges
299 the gap of tracing, by using unique nomenclature and managing hundreds of graphical outputs
300 in a logical approach.

301 Use cases

302 Assessment and validation of individual neurons

303 In [26, 28], we reported the presence of spatially-responsive neurons in the rat anterior and
304 rostral thalamic nuclei. Consider one of the place cells as shown in Figure 6 [37]. The top and
305 middle row show where in the environment one such unit becomes active (spike-plot) and the
306 firing rate map of the unit with respect to the 2D location of the animal. The patch of high
307 firing zone implies that the unit is responsive to the location of the animal. This patch of firing
308 could result from three different factors:

- 309 1. The unit may fire with respect to that part of the border, as in boundary vector cells [13].

-
- 310 2. The animal might face the north wall of the environment while approaching that area and
311 a head directional unit may appear as a place cell, because of constraints on the trajectory
312 of movement, and therefore of the sampling of unit activity (Figure 6; bottom).
- 313 3. The unit might also be a head direction-by-place cell, where the unit fires in a certain
314 location of the environment only when it is heading towards a particular direction [8].

315 We can use multiple built-in analysis methods in NeuroChaT to assess and confirm whether
316 the unit is a place cell as mentioned below:

- 317 1. Multiple regression analysis models the instantaneous firing rate of the unit by a linear
318 combination of the environmental variables under consideration [5] and provides the
319 relative contribution of each factor on the firing property of the unit. As the firing rates
320 are idiosyncratic for place and head-directional cells, the variable values were replaced by
321 the corresponding average firing rate maps.
- 322 2. Assuming the null hypothesis that the observation of a place cell is a matter of chance,
323 we can do shuffling analysis. In this technique, neuronal spikes are randomly shuffled
324 and the specificity index (Skaggs Information Content) [3] for each such artificial unit is
325 calculated. The specificity index of the unit is tested whether it is significantly larger than
326 the mean information content in a population of shuffled simulated units firing randomly
327 with respect to the location.
- 328 3. Finally, we can perform the time-shift analysis and observe whether the unit follows
329 a gradual change in information content with respect to the time-shift, implying that
330 the firing rate is not random, and there is a consistent and graded, or a systematic
331 location-related variation.

332 The multiple regression for this unit (Figure 6b) shows that the variation in spiking activity
333 is primarily due to the location of the animal and is not merely due to other factors. Skaggs
334 distribution shows that the information calculated from the original spiking activity is greater
335 than 95th percentile of the distribution in random spiking, implying that the specificity to
336 locational firing is significantly larger than the randomly-correlated units and, therefore, the null
337 hypothesis of observing the locational firing of the unit by chance is not true. The time shift
338 analysis, although not very smooth, still shows that there is a graded change in the information
339 content, marked by the parabolic change in information content as the timing of the unit-activity
340 is gradually shifted by -200 ms to 400 ms, which further implies that the effect of location on
341 the firing rate is systematic rather than random.

342 **Assessment and validation of a population of neurons**

343 The analysis outcome in NeuroChaT has been used to assess the effect of stress induced by
344 high-intensity light exposure to rats on its spatial information processing system, particularly
345 on units that represent the head-directional information in postsubiculum of the hippocampal
346 formation (HF) [36]. Following the initial cell selection, 230 units were analysed using NeuroChaT
347 [37]. The units with dominant head-directional firing were identified using supervised k-means
348 clustering of the distribution of multiple-regression coefficients (Figure 7a) for location and
349 head-direction. We did not find significant correlations for border angular head-velocity and
350 running speed of the animal. Sixty-five head-directional (HD) cells were identified to be in a
351 distinct cluster, representing higher correlation to direction. Several of NeuroChaT's numerical
352 outputs such as the preferred firing direction of the HD cells and the peak firing rate were
353 used for characterising the units and comparing the changes in these characteristics due to
354 stress. Each unit remained a stable predictor of direction in both the conditions as the preferred
355 head-directionality of units remained unaffected (Figure 7b; Pearson's $r^2 = 0.64, p < 0.001$)
356 and the accuracy of directional representation, as measured by the half-width of the directional

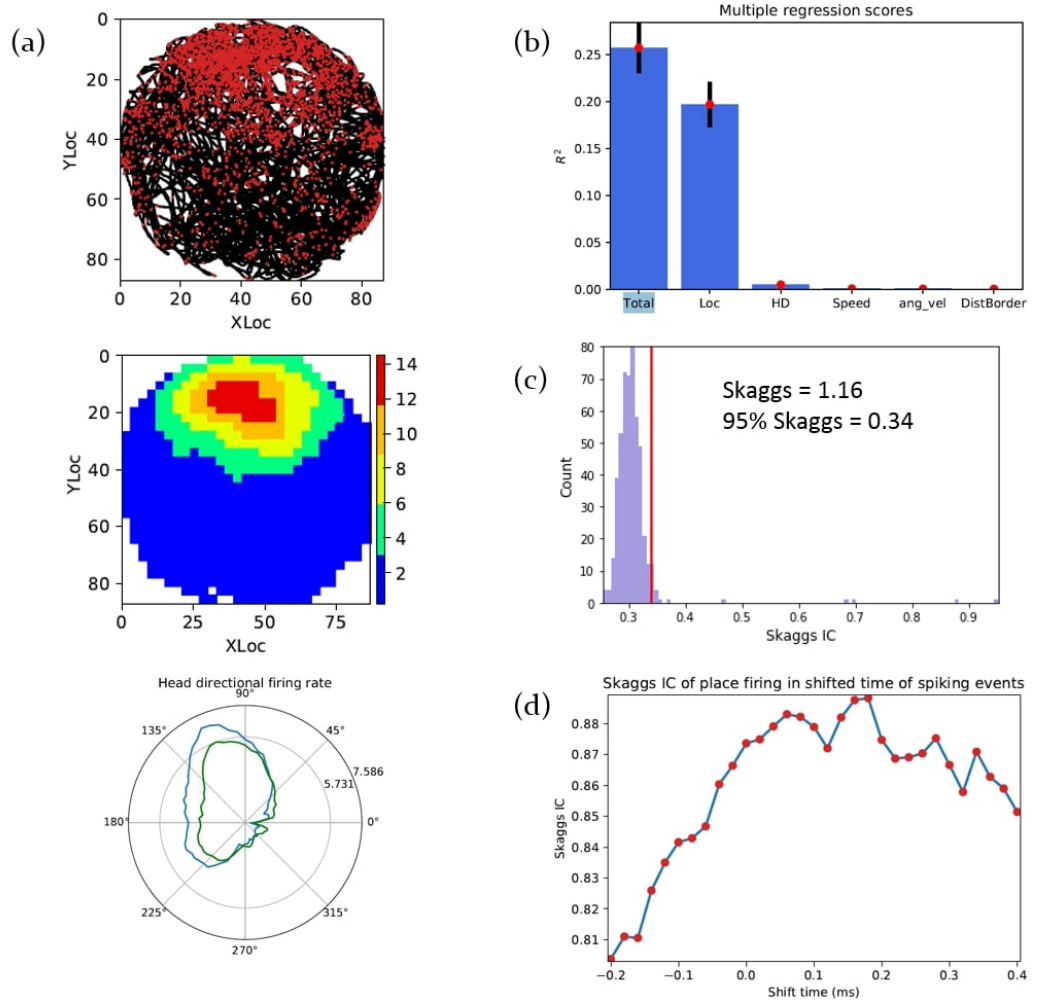


Figure 6. Identifying and verifying a place cell using analyses in NeuroChaT recorded in rat anterior thalamus [28]. (a) Top- the scatter plot of spiking-activity showing the path of the animal (black line) and the location in the arena where spiking activity occurred (red dots); Middle- the firing rate map of the unit showing the patch of locational receptive field. These two plots provide the initial screening of the place unit. Bottom- the firing rate of the unit with respect to the head-direction of the animal. The blue line shows the true rate and the green line is the predicted rate as described by Cacucci *et al.* [8]. Both lines are very similar, implying that there is a sampling bias for the head-direction and, therefore, the tuned rate towards nearly north direction is not representative of the head-directional unit. (b) Multiple regression analysis shows that location contributes to most of the variation in firing rate, confirming that the location is the main contributing factor and, in this case, the only factor to contribute to the spiking activity. (c) The distribution of Skaggs in randomly shuffled spike time (no. of shuffles = 500). The 95th percentile (0.34) of the distribution is much lower than the Skaggs of the original activity of the unit (1.16), so the place cell activity is not random. (d) The systematic changes in Skaggs information content (IC) as spiking timing is shifted by -0.2 s to 0.4 s in steps of 25 ms.

357 tuning curve was unaltered (Pearson's $r^2 = 0.715, p < 0.001$). Head-directional partial r values
358 and peak head-directional firing rate variables showed a significant decrease in value (Figure 7c
359 and d; mean head-directional partial r value $Z65 = -3.029, p = 0.002$, peak head-directional
360 rate $Z65 = -2.109, p = 0.035$). A number of other aspects were also studied, such as assessing
361 whether the photic stress influences a specific sub-population of head-direction cells, see Figure 7
362 (adapted from [36]).

363 **Assessment of rhythmic properties of a neuron**

364 Spike-train dynamics and the nature of the interaction with simultaneously recorded LFP
365 provides vital information to understand the neuronal networks and the dynamics of individual
366 neural components across different brain areas [18, 23]. Analysis of this sort can be important
367 particularly for assessing the mechanism of spatial computation as it is hypothesised that there
368 is a spatial information packaging by theta rhythms [24]. The cortical head-directional cells
369 are segregated in time by alternating theta cycles according to their directional preference
370 [23], hippocampal place cells show location specific phase-segregation reflecting the distance
371 representation by time-compression, which is also dependent on speed of the animal [11], and
372 separate theta cycles segregate distinct environmental representations and the changes in context,
373 i.e. location of reward [18]. Analysis of theta-modulated units, theta-skipping units, and units
374 to LFP phase synchrony are widely used in this regard. In NeuroChaT, we assess them using
375 the following analyses:

- 376 1. The distribution of ISI, and the relationship of the interval before vs interval after.
- 377 2. The autocorrelation histogram of ISI, which exfoliates the rhythmic pattern merely observed
378 for the ISI itself.
- 379 3. The distribution of LFP-phases at the time of the unit activity [10], the phase-locking
380 value (PLV) [17] and the spike-field coherence (SFC) [16] at different frequencies.

381 A unit with clear rhythmicity in firing activity represented by a higher count of ISI at
382 around 125 ms is shown in the upper row of Figure 8 [37]. This unit was co-recorded with
383 head-directional cells in the electrophysiology study of thalamic nuclei [26, 28]. The scatter plot
384 of ISI before and after shows distinct patches implying the replication of ISI at those values
385 (roughly 125 ms). The autocorrelation histogram unfolds the rhythmicity more prominently.
386 As the replication occurs at around 8 Hz or in the Theta-rhythmic band, this unit is called a
387 theta-modulated cell. Further analysis of this unit provides its descriptive characteristics.
388 The spike to LFP phase distribution shows that there is a higher count of phases at around
389 195° . Although the delta band signal dominates the underlying LFP, the unit is still strongly
390 locked to the theta-band as can be seen from the high PLV and SFC at around 10 Hz. The
391 time-resolved PLV and SFC analysis of the unit provides further insight into the temporal nature
392 of the locking. As the bottom row of Figure 8 shows, the locking is maximal at around 10 Hz
393 throughout the entire window, but it evolves after the spiking event and maximises at a lag of
394 roughly 125 ms, implying that the theta phase encodes the spiking event. One interpretation of
395 the 125 ms lag for maximal locking is that the spiking event is encoded in the next cycle of the
396 theta wave.

397 **Discussion**

398 We developed the NeuroChaT toolbox to facilitate and standardise the analysis of neuronal spike
399 trains and their relationship to behaviour and to simultaneously recorded LFP signals. Neu-
400 roChaT is hosted in a GitHub repository (<https://github.com/shanemomara/omaraneurolab>).
401 We provide a simple graphical interface and an easy-to-use API for using the corresponding
402 analysis techniques and managing data. We hope that providing a simple, easy to use software

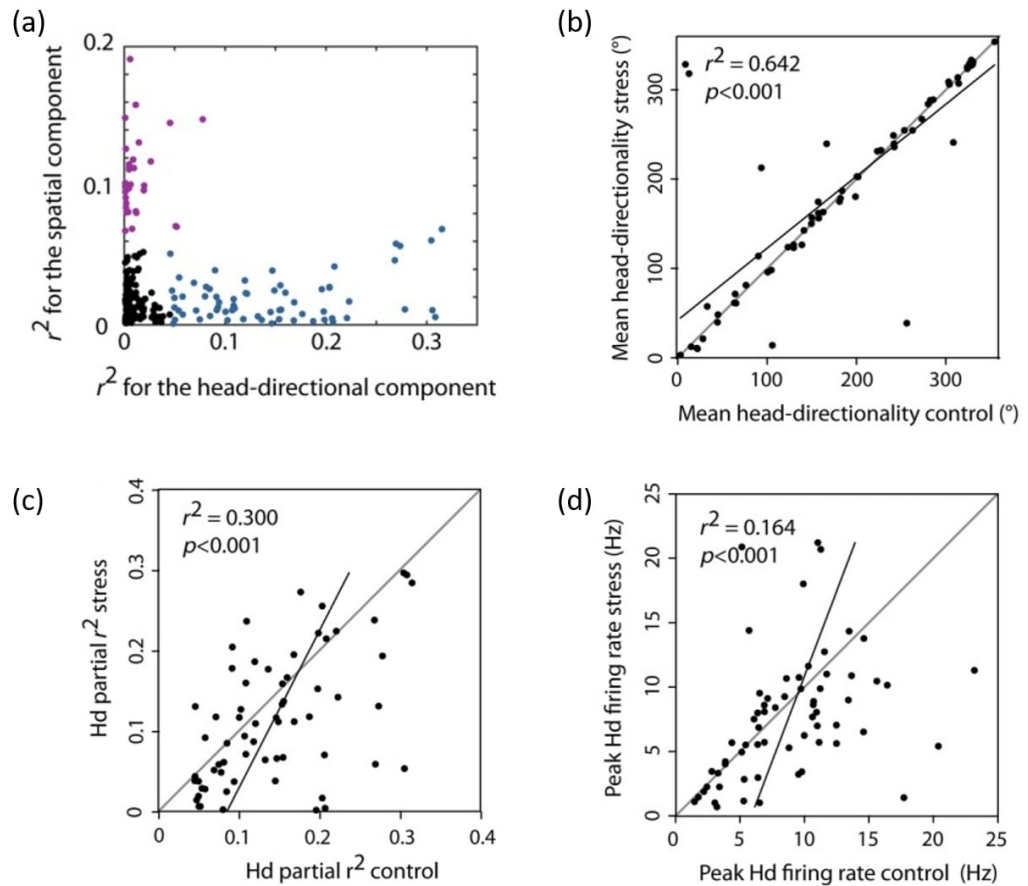


Figure 7. Study of the effect of photic stress on postsubicular head-directional cells (adapted from [36]). NeuroChaT output parameters were used to accomplish the study. a) Identification of head-directional cells of recorded postsubicular cells. Correlation coefficients from multiple linear regression analysis and subsequent cluster-analysis revealed spatial (purple) and head-directional (blue) cells. The head-directional cells are not changing their preferred direction of firing, as shown by the high correlation between the mean directions of the neurons before and after stress induction (b), but the correlation coefficient representing the variability of the firing rates due to head-direction (c) and the peak firing rates (d) changes. This implies that information processing is disrupted due to stress experienced by the rats.

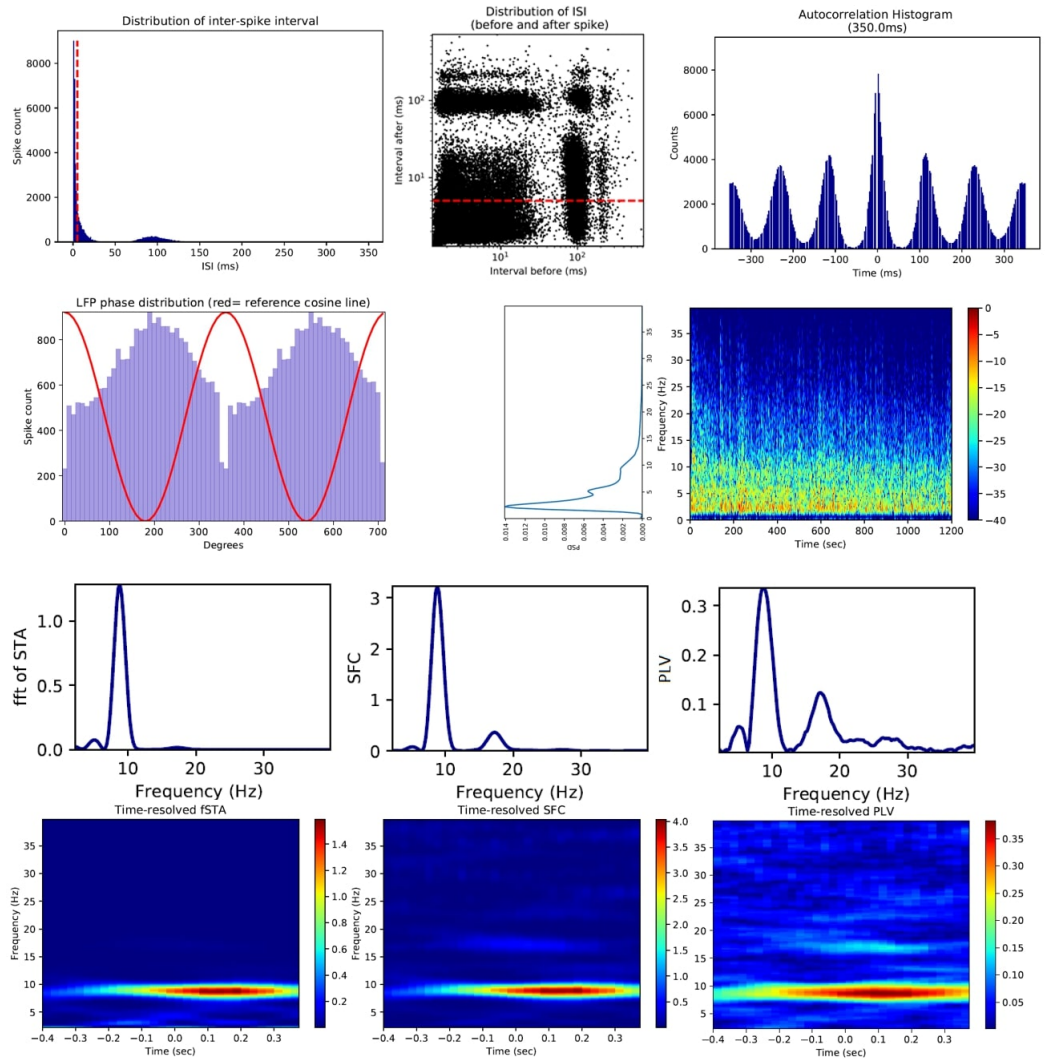


Figure 8. Upper row: left- inter-spike interval (ISI) distribution revealing that this unit has high burst propensity and is theta-rhythmic; middle- ISI before vs after discloses the characteristic patches at around 125 ms indicating high replication of such ISI events; right- autocorrelation of ISI histogram amplifies the rhythmic effect. Middle row: left- distribution of spike phases with underlying local field potential (LFP) signal; right- LFP power spectrum showing that there is a presence of weak theta-rhythm in the LFP. Lower row: although the LFP theta is small, the frequency spectrum of spike-triggered average (STA; left), the spike-field coherence (SFC; middle) and phase-locking value (PLV; right) all display strong locking to theta signal, verifying the locking as seen in phase distribution. Bottom row: the time-resolved fast Fourier transform (FFT) of STA (left), SFC (middle), and PLV (right) show that the peak locking does not occur simultaneously and has a lag from the time of spike-onset. It may imply that the LFP phase is encoding the spiking event instead of momentary representation or prediction of the spikes. The lag time for peak metric is 125 ms, which may also imply that the spiking event is represented in the next theta cycle instead of the synchronous one.

403 package will facilitate the adoption of *in vivo* recording techniques. We hope that NeuroChaT,
404 by assembling standard analyses techniques in one place along with a standard workflow will
405 facilitate the adoption of standardised analyses for behavioural neurophysiology, and facilitate
406 open data sharing and collaboration between laboratories. The simple GUI is designed for
407 researchers without programming knowledge, while the versatile design in API provides an
408 opportunity for neuroscientists with programming expertise to use the platform as a starting
409 tool for extending their analytic capabilities. The built-in collection of analyses methods will
410 allow them to quickly scan and infer the characteristics of the recorded neurons and refine their
411 experimental protocols. The examples both here and in the project documentation depict how
412 NeuroChaT can be used to build a custom analysis portfolio for characterising single units and
413 population of neurons.

414 Some commercial and open-source toolboxes, such as Neo [25], support conversion of electro-
415 physiology data from several copyrighted formats (i.e. Axona, Blackrock, Plexon, NeuroExplorer
416 etc.) to HDF5 format. NeuroChaT currently supports Axona and NeuroLynx formats. Integrat-
417 ing other data formats will be useful to provide for the analytic need of scientists using recording
418 systems from a wide range of vendors. Currently, NeuroChaT supports analyses that pertain to
419 assessing the dynamics of spatial correlates of neuronal responses. Analysis of stimulus-response
420 dynamics is also widely studied in neurophysiology. Extensive development of event-related
421 analysis using both the LFP and single-unit data will potentially open the door for wide-spread
422 reception among neurophysiologists. An effort to integrate or to interface popular automated
423 spike sorting algorithms or toolboxes can also be undertaken. Although there are frameworks
424 for LFP-LFP [14] and point-process causality analysis between spike-trains [20], as far as we
425 are aware, there is no such framework for studying the causal relations between the spike-train
426 of a unit and simultaneously recorded LFP signals. Future work will pursue this aspect of
427 analysis as well. Owing to the rise of big data in neurophysiology and envisioning the use of
428 cloud computing [32], future developments of NeuroChaT can target a cloud-native version to
429 support distributed computing and work with algorithms to support such technologies.

430 Data availability

431 *Underlying data*

432 Open Science Framework: NeuroChaT: Neuron Characterization Toolbox.
433 DOI: <https://doi.org/10.17605/OSF.IO/642YH> [37].

434 This project contains the following underlying data:

- 435 • Example Place cell: 040513.1.hdf5 (Assessment and validation of individual neurons -
436 neuronal data to reproduce Figure 6. This data was recorded by Maciej Jankowski [28].)
- 437 • Data from Passecker et al 2018.xlsx (Assessment and validation of a population of neurons -
438 spreadsheet data containing the numerical output from NeuroChaT used to create Figure 7
439 (adapted from [36]). This data was collected by Johannes Passecker [36])
- 440 • Example theta modulated cell_conjunctive speed cell: 112512.1.hdf5 (Assessment of
441 rhythmic properties of a neuron - neuronal data to reproduce Figure 8. This data was
442 recorded by Maciej Jankowski [26, 28].)

443 *Extended data*

444 Open Science Framework: NeuroChaT: Neuron Characterization Toolbox.
445 DOI: <https://doi.org/10.17605/OSF.IO/642YH> [37]

446 This project contains the following extended data:

- 447 • Example Border cell: 040114.C3.hdf5 (recorded by Paul Wynne).
- 448 • Example Gradient cell: conjunctive angular head velocity and speed cell: 052214.C1.hdf5
449 (recorded by Paul Wynne).
- 450 • Example Grid cell: 120213.26.hdf5 (recorded by Maciej Jankowski).
- 451 • Example Head Directional cell: 120412.1.hdf5 (recorded by Maciej Jankowski).

452 Data are available under the terms of the Creative Commons Zero "No rights reserved" data
453 waiver (CC0 1.0 Public domain dedication).

454 Software availability

- 455 • An executable version of NeuroChaT for non-coder Windows users is available from: <https://github.com/shanemomara/omaraneurolab/releases/download/v1.1.0/NeuroChaT.exe>
456
- 457 • Source code available from: <https://github.com/shanemomara/omaraneurolab/tree/master/NeuroChaT>
458
- 459 • Archived source code at time of publication: <https://doi.org/10.5281/zenodo.3543732>
- 460 • License: GNU General Public License version 3

461 Competing interests

462 No competing interests were disclosed.

463 Grant information

464 This work was supported by the Wellcome Trust through a Joint Senior Investigator Award to
465 JP Aggleton and SM O'Mara [103723].

466 *The funders had no role in study design, data collection and analysis, decision to publish, or*
467 *preparation of the manuscript.*

468 Acknowledgements

469 We thank Paul Wynne, Pawel Matulewicz, Beth Frost, Katharina Ulrich, Emanuela Rizzello,
470 Johannes Passecker, Matheus Cafalchio and Maciej Jankowski for comments and feedback on

472 **References**

- 473 1. O’Keefe, J. & Dostrovsky, J. The hippocampus as a spatial map. Preliminary evidence
474 from unit activity in the freely-moving rat. eng. *Brain Res.* **34**, 171–175. ISSN: 0006-8993
475 (Nov. 1971).
- 476 2. Taube, J. S., Muller, R. U. & Ranck, J. B. Head-direction cells recorded from the post-
477 subiculum in freely moving rats. I. Description and quantitative analysis. eng. *J. Neurosci.*
478 **10**, 420–435. ISSN: 0270-6474 (Feb. 1990).
- 479 3. Skaggs, W. E., McNaughton, B. L. & Gothard, K. M. *An Information-Theoretic Approach to*
480 *Deciphering the Hippocampal Code in Advances in Neural Information Processing Systems*
481 *5, [NIPS Conference]* (Morgan Kaufmann Publishers Inc., San Francisco, CA, USA, 1993),
482 1030–1037. ISBN: 978-1-55860-274-8. [http://dl.acm.org/citation.cfm?id=645753.](http://dl.acm.org/citation.cfm?id=645753.668057)
483 668057 (2019).
- 484 4. Gamma, E., Helm, R., Johnson, R. & Vlissides, J. *Design Patterns: Elements of Reusable*
485 *Object-oriented Software* ISBN: 978-0-201-63361-0 (Addison-Wesley Longman Publishing
486 Co., Inc., Boston, MA, USA, 1995).
- 487 5. Sharp, P. E. Multiple spatial/behavioral correlates for cells in the rat postsubiculum:
488 multiple regression analysis and comparison to other hippocampal areas. eng. *Cereb.*
489 *Cortex* **6**, 238–259. ISSN: 1047-3211 (Apr. 1996).
- 490 6. Sharp, P. E. Comparison of the timing of hippocampal and subicular spatial signals:
491 implications for path integration. eng. *Hippocampus* **9**, 158–172. ISSN: 1050-9631 (1999).
- 492 7. Bassett, J. P. & Taube, J. S. Neural correlates for angular head velocity in the rat dorsal
493 tegmental nucleus. eng. *J. Neurosci.* **21**, 5740–5751. ISSN: 1529-2401 (Aug. 2001).
- 494 8. Cacucci, F., Lever, C., Wills, T. J., Burgess, N. & O’Keefe, J. Theta-modulated place-by-
495 direction cells in the hippocampal formation in the rat. eng. *J. Neurosci.* **24**, 8265–8277.
496 ISSN: 1529-2401 (Sept. 2004).
- 497 9. Hafting, T., Fyhn, M., Molden, S., Moser, M.-B. & Moser, E. I. Microstructure of a
498 spatial map in the entorhinal cortex. en. *Nature* **436**, 801–806. ISSN: 1476-4687. <https://www.nature.com/articles/nature03721> (2019) (Aug. 2005).
- 500 10. Siapas, A. G., Lubenov, E. V. & Wilson, M. A. Prefrontal phase locking to hippocampal
501 theta oscillations. eng. *Neuron* **46**, 141–151. ISSN: 0896-6273 (Apr. 2005).
- 502 11. Geisler, C., Robbe, D., Zugaro, M., Sirota, A. & Buzsáki, G. Hippocampal place cell
503 assemblies are speed-controlled oscillators. en. *PNAS* **104**, 8149–8154. ISSN: 0027-8424,
504 1091-6490. <https://www.pnas.org/content/104/19/8149> (2019) (May 2007).
- 505 12. Moser, E. I., Kropff, E. & Moser, M.-B. Place cells, grid cells, and the brain’s spatial
506 representation system. eng. *Annu. Rev. Neurosci.* **31**, 69–89. ISSN: 0147-006X (2008).
- 507 13. Lever, C., Burton, S., Jeewajee, A., O’Keefe, J. & Burgess, N. Boundary Vector Cells
508 in the Subiculum of the Hippocampal Formation. en. *J. Neurosci.* **29**, 9771–9777. ISSN:
509 0270-6474, 1529-2401. <https://www.jneurosci.org/content/29/31/9771> (2019) (Aug.
510 2009).
- 511 14. Cadotte, A. J. *et al.* Granger Causality Relationships between Local Field Potentials in
512 an Animal Model of Temporal Lobe Epilepsy. *J Neurosci Methods* **189**, 121–129. ISSN:
513 0165-0270. <https://www.ncbi.nlm.nih.gov/pmc/articles/PMC2867107/> (2019) (May
514 2010).

-
- 515 15. Ince, R. A. A., Mazzoni, A., Petersen, R. S. & Panzeri, S. Open source tools for the
516 information theoretic analysis of neural data. eng. *Front Neurosci* **4**. ISSN: 1662-453X
517 (2010).
- 518 16. Rutishauser, U., Ross, I. B., Mamelak, A. N. & Schuman, E. M. Human memory strength
519 is predicted by theta-frequency phase-locking of single neurons. en. *Nature* **464**, 903–907.
520 ISSN: 1476-4687. <https://www.nature.com/articles/nature08860> (2019) (Apr. 2010).
- 521 17. Van Wingerden, M., Vinck, M., Lankelma, J. & Pennartz, C. M. A. Theta-band phase
522 locking of orbitofrontal neurons during reward expectancy. eng. *J. Neurosci.* **30**, 7078–7087.
523 ISSN: 1529-2401 (May 2010).
- 524 18. Jezek, K., Henriksen, E. J., Treves, A., Moser, E. I. & Moser, M.-B. Theta-paced flickering
525 between place-cell maps in the hippocampus. en. *Nature* **478**, 246–249. ISSN: 1476-4687.
526 <https://www.nature.com/articles/nature10439> (2019) (Oct. 2011).
- 527 19. Stevenson, I. H. & Kording, K. P. How advances in neural recording affect data analysis. en.
528 *Nature Neuroscience* **14**, 139–142. ISSN: 1546-1726. <https://www.nature.com/articles/nn.2731> (2019) (Feb. 2011).
- 530 20. Cajigas, I., Malik, W. Q. & Brown, E. N. nSTAT: open-source neural spike train analysis
531 toolbox for Matlab. eng. *J. Neurosci. Methods* **211**, 245–264. ISSN: 1872-678X (Nov. 2012).
- 532 21. Quiroga, R. Q. Spike sorting. eng. *Curr. Biol.* **22**, R45–46. ISSN: 1879-0445 (Jan. 2012).
- 533 22. Alivisatos, A. P. *et al.* Nanotools for Neuroscience and Brain Activity Mapping. *ACS*
534 *Nano* **7**, 1850–1866. ISSN: 1936-0851. [https://www.ncbi.nlm.nih.gov/pmc/articles/](https://www.ncbi.nlm.nih.gov/pmc/articles/PMC3665747/)
535 [PMC3665747/](https://www.ncbi.nlm.nih.gov/pmc/articles/PMC3665747/) (2019) (Mar. 2013).
- 536 23. Brandon, M. P., Bogaard, A. R., Schultheiss, N. W. & Hasselmo, M. E. Segregation of
537 cortical head direction cell assemblies on alternating theta cycles. en. *Nature Neuroscience*
538 **16**, 739–748. ISSN: 1546-1726. <https://www.nature.com/articles/nn.3383> (2019) (June
539 2013).
- 540 24. Colgin, L. L. Mechanisms and functions of theta rhythms. eng. *Annu. Rev. Neurosci.* **36**,
541 295–312. ISSN: 1545-4126 (July 2013).
- 542 25. Garcia, S. *et al.* Neo: an object model for handling electrophysiology data in multiple
543 formats. English. *Front. Neuroinform.* **8**. ISSN: 1662-5196. [https://www.frontiersin.](https://www.frontiersin.org/articles/10.3389/fninf.2014.00010/full)
544 [org/articles/10.3389/fninf.2014.00010/full](https://www.frontiersin.org/articles/10.3389/fninf.2014.00010/full) (2019) (2014).
- 545 26. Jankowski, M. M. *et al.* Nucleus reuniens of the thalamus contains head direction cells. *eLife*
546 **3** (ed Eichenbaum, H.) e03075. ISSN: 2050-084X. <https://doi.org/10.7554/eLife.03075>
547 (2019) (July 2014).
- 548 27. Jankowski, M. M. & O'Mara, S. M. Dynamics of place, boundary and object encoding in
549 rat anterior claustrum. eng. *Front Behav Neurosci* **9**, 250. ISSN: 1662-5153 (2015).
- 550 28. Jankowski, M. M. *et al.* Evidence for spatially-responsive neurons in the rostral thalamus.
551 eng. *Front Behav Neurosci* **9**, 256. ISSN: 1662-5153 (2015).
- 552 29. Kropff, E., Carmichael, J. E., Moser, M.-B. & Moser, E. I. Speed cells in the medial
553 entorhinal cortex. eng. *Nature* **523**, 419–424. ISSN: 1476-4687 (July 2015).
- 554 30. Rey, H. G., Pedreira, C. & Quiroga, R. Past, present and future of spike sorting
555 techniques. eng. *Brain Res. Bull.* **119**, 106–117. ISSN: 1873-2747 (Oct. 2015).
- 556 31. Teeters, J. L. *et al.* Neurodata Without Borders: Creating a Common Data Format for
557 Neurophysiology. eng. *Neuron* **88**, 629–634. ISSN: 1097-4199 (Nov. 2015).
- 558 32. Bouchard, K. E. *et al.* High-Performance Computing in Neuroscience for Data-Driven
559 Discovery, Integration, and Dissemination. eng. *Neuron* **92**, 628–631. ISSN: 1097-4199 (Nov.
560 2016).

-
- 561 33. Mahmud, M. & Vassanelli, S. Processing and Analysis of Multichannel Extracellular
562 Neuronal Signals: State-of-the-Art and Challenges. English. *Front. Neurosci.* **10**. ISSN: 1662-
563 453X. <https://www.frontiersin.org/articles/10.3389/fnins.2016.00248/full>
564 (2019) (2016).
- 565 34. Grieves, R. M. & Jeffery, K. J. The representation of space in the brain. *Behavioural*
566 *Processes* **135**, 113–131. ISSN: 0376-6357. [http://www.sciencedirect.com/science/](http://www.sciencedirect.com/science/article/pii/S0376635716302480)
567 [article/pii/S0376635716302480](http://www.sciencedirect.com/science/article/pii/S0376635716302480) (2019) (Feb. 2017).
- 568 35. Jun, J. J. *et al.* Fully integrated silicon probes for high-density recording of neural ac-
569 tivity. en. *Nature* **551**, 232–236. ISSN: 1476-4687. [https://www.nature.com/articles/](https://www.nature.com/articles/nature24636)
570 [nature24636](https://www.nature.com/articles/nature24636) (2019) (Nov. 2017).
- 571 36. Passecker, J., Islam, M. N., Hok, V. & O’Mara, S. M. Influences of photic stress on
572 postsubicular head-directional processing. eng. *Eur. J. Neurosci.* **47**, 1003–1012. ISSN:
573 1460-9568 (Apr. 2018).
- 574 37. Islam, M. N., Martin, S. K. & O’Mara, S. *NeuroChaT: Neuron Characterization Toolbox*
575 2019. osf.io/642yh.